

Cite this: *J. Mater. Chem. A*, 2023, 11, 7179

Surface fully functionalized metal chalcogenide nanowires for highly sensitive H₂S sensing†

Ying-Xue Jin,^{ad} Jie Chen,^{ac} Yong-Jun Chen,^a Wei-Hua Deng,^a Xiao-Liang Ye,^a Guan-E Wang^{id} *^{ad} and Gang Xu^{id} *^{abd}

Modifiable one-dimensional materials are extremely desired in various applications, especially in room-temperature (RT) chemiresistive gas sensing. New one-dimensional (1D) CdS-based metal chalcogenide nanowires with a surface fully covered amino group (denoted as Cd-ATP) were prepared by the coordination self-assembly method. Featuring densely covered organic functional motifs, Cd-ATP is able to selectively recognize H₂S through hydrogen bonding interaction between the amino group and H₂S. Cd-ATP exhibits high sensitivity, an ultra-low limit-of-detection (116.49 ppt) and fast response/recovery among all reported room temperature H₂S sensing non-composite materials. This work provides inspiration for the design and preparation of novel surface fully functionalized 1D materials for various chemical applications.

Received 20th January 2023
Accepted 1st March 2023

DOI: 10.1039/d3ta00377a

rsc.li/materials-a

Introduction

Semiconductive nanowires, with a large aspect ratio and specific surface area, are an important class of nanostructure building blocks. The confinement effect endows them with unique properties different from traditional bulk materials and displays potential applications in photochemistry, catalysis, optoelectronics, supercapacitors, batteries, and chemical sensors.^{1–6} Increasing the number of facial active sites could further optimize the properties of the semiconductor nanowires. An effective method is to graft functional organic groups onto the nanowires by post-modification through covalent or coordination bonds.^{7–10} For example, amino functional groups can be grafted onto a In₂O₃ nanowire surface by soaking it in 3-(trimethoxysilyl)propyl aldehyde for selective identification of antibodies.¹¹ Wang *et al.* used the aminosilane reagent ([1-(2-amino-ethyl)-3-aminopropyl]trimethoxysilane (AAPTS)) to functionalize a titanate nanowire and improve its Cr(VI) adsorption properties.^{12,13} Chen *et al.* reported a CdS single-crystalline nanowire sensor to detect 100 ppm H₂S with a response value of 20%,¹⁴ and this value can be increased to 75% when modified

with polyaniline.¹⁵ However, the number of organic functional groups grafted by these post-modified methods is uncertain and the distribution is disordered. Additionally, post-modified methods may hinder the application of the materials.

Coordination self-assembly is an effective way to construct ordered structures between metal ions and organic ligands through coordination or covalent bonds. Ordered arrangement of customized functional groups can embellish the surface of inorganic nanowires or layers by this method. An emerging class of nanomaterials with a fully functionalized surface, 2D organic metal chalcogenides (OMCs), have been successfully prepared by this method recently. Moreover, the band gap, conductivity, catalytic and sensing properties can be greatly regulated by adjusting the types of functional groups on the surface of OMCs.^{16–20} Inspired by 2D OMCs, it is also possible for nanowires to functionalize in this way. However, few examples of such nanowires have been developed by this method, and their application in devices is still rare.^{21,22}

In this work, a novel amino homogeneously modified one-dimensional metal chalcogenide nanowire, Cd-ATP (ATP = 4-aminothiophenol), was fabricated by the coordination self-assembly method. The amino group was covalently connected to the *para*-C atom of the thiol ligand, thereby realizing a fully and ordered covered organic group at the molecular level. In order to expose more organic functional groups, nanowires with a diameter of ~25 nm were synthesized by the ultrasonic method. Moreover, a nanowire mesh film of Cd-ATP was prepared by vacuum filtration for chemical resistance sensors, which show a high sensitivity, fast response time, excellent selectivity, and lowest limit of detection (LOD) under visible light compared with other conventional RT H₂S-sensing materials.

^aState Key Laboratory of Structural Chemistry, Fujian Institute of Research on the Structure of Matter, Chinese Academy of Sciences, Fuzhou, Fujian 350002, China. E-mail: gewang@fjirsm.ac.cn; gxu@fjirsm.ac.cn

^bScience & Technology Innovation Laboratory for Optoelectronic Information of China, Fuzhou, Fujian 350108, China

^cCollege of Chemistry, Fuzhou University, Fuzhou, Fujian 350116, China

^dUniversity of Chinese Academy of Sciences (UCAS), Beijing 100049, China

† Electronic supplementary information (ESI) available: Experimental details and characterization data as well as the crystallographic data of Cd-ATP. CCDC 2235334. For ESI and crystallographic data in CIF or other electronic format see DOI: <https://doi.org/10.1039/d3ta00377a>

Results and discussion

A colorless spindle Cd-ATP crystal was synthesized by coordination assembly of Cd^{2+} ions and 4-aminothiophenol through the solvothermal method (Fig. 1a, more details shown in the ESI†). The crystal structure was determined by X-ray diffraction and revealed that Cd-ATP crystallizes in a triclinic space group, $P\bar{1}$ (see Fig. S2, Tables S1 and S2†). As shown in Fig. 1b, all Cd is coordinated by four S atoms to form a slightly distorted tetrahedral configuration. The tetrahedra are connected to each other through edge-sharing to form a Cd_4S_9^- cluster. Such a Cd_4S_9^- cluster is further connected by two K^+ to form a 1D nanowire. The amino group covered the surface of the nanowire through covalent connection to the *para*-C atom of the thiol ligand (Fig. 1c). And the nanowires are connected by van der Waals forces to form a complete three-dimensional structure (Fig. 1d).

The powder X-ray diffraction patterns of the synthesized Cd-ATP nanowires (see the ESI†) are in good agreement with the simulated pattern from single crystal X-ray diffraction (Fig. 1e), indicating that Cd-ATP nanowires have fine crystallinity and high purity. Besides, Cd-ATP nanowires were further characterized by X-ray photoelectron spectroscopy (XPS) (Fig. S3†) and Fourier-transform infrared (FT-IR). Concretely, the peaks for N–H stretching vibration (3378 and 3306 cm^{-1}) are observed in the FT-IR spectrum (Fig. 1f), which show the existence of uncoordinated amino groups of Cd-ATP. Moreover, the binding energy of N 1s is confirmed to be 399.5 eV by XPS measurement (Fig. 1g), which is the same as that of phenylamine,²³ further indicating the non-coordinated amino group. These uncoordinated amino groups can provide the active sites for selectively recognising foreign molecules.

Numerous efforts have been made to use both the size and surface effects of the nanoscale materials to enhance the performance of materials. Nanoscale materials with semiconductor characteristics and high stability may be conducive to electrical devices.^{24–28} Cd-ATP nanowires with a diameter of

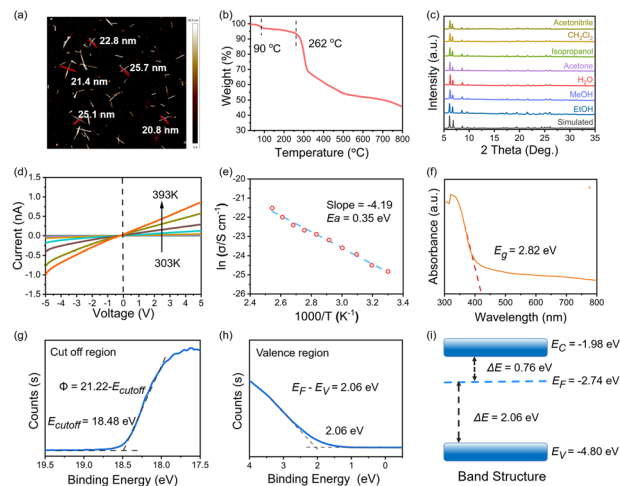


Fig. 2 Basic characterization of Cd-ATP nanowires. (a) AFM image of Cd-ATP nanowires. (b) TG curve of Cd-ATP nanowires (c) PXRD patterns after immersion in different organic solvents for 7 days. (d) Variable temperature conductivity of Cd-ATP nanowires. (e) Fitting of conductivity–temperature data to the Arrhenius equation. (f) UV-vis absorbance spectrum of Cd-ATP nanowires. (g) The secondary electron cut off of Cd-ATP nanowires measured with He I ($h\nu = 21.22\text{ eV}$). (h) Valence band of Cd-ATP nanowires with respect to the Fermi level ($E_F = 0$). (i) Band structure diagram of Cd-ATP nanowires.

about 25 nm (Fig. 2a) were synthesized by ultrasound methods. Meanwhile, Cd-ATP nanowires maintain good thermal stability up to 262 °C (Fig. 2b) and chemical stability by immersion in different organic solvents for 7 days (Fig. 2c). To further explore the semiconductor properties of the material, the conductivity of Cd-ATP nanowires is $7.90 \times 10^{-11}\text{ S cm}^{-1}$ at RT obtained by the standard two-contact probe method measurement, which increased with the increase of temperature (Fig. 2d), indicating its typical semiconductor characteristics with an activation energy of 0.35 eV (Fig. 2e). According to the UV-vis absorption spectrum, the band gap of Cd-ATP is 2.82 eV (Fig. 2f). UPS is performed to determine the electronic structure of Cd-ATP nanowires. The Fermi energy level is calculated to be -2.74 eV from the work functions ($\phi = 21.22 - E_{\text{cutoff}}$) (Fig. 2g). As shown in Fig. 2h, the valence band is 2.06 eV below the Fermi level (E_F) with a value of -4.80 eV . Combining the valence band spectrum with an optical band gap obtained from UV-vis spectroscopy (Fig. 2f), the conduction band is derived to be -1.98 eV (Fig. 2i). The Fermi level (E_F) of Cd-ATP nanowires is closer to the conduction band, suggesting that it is an N-type semiconductor.

In recent years, the detection of toxic and hazardous gases at room temperature has attracted considerable attention due to human health problems and increasing environmental pollution.^{29–31} Metal chalcogenides have been widely used in the field of gas sensors due to their unique electronic properties and excellent physicochemical properties.^{32–35} The semi-conducting properties, high specific surface area and high stability of Cd-ATP have attracted much attention as conductive gas sensors. To further better apply Cd-ATP nanowires to chemiresistive gas sensing, a Cd-ATP nanowire mesh film (Fig. 3b) was fabricated by vacuum filtration as shown in Fig. 3a.

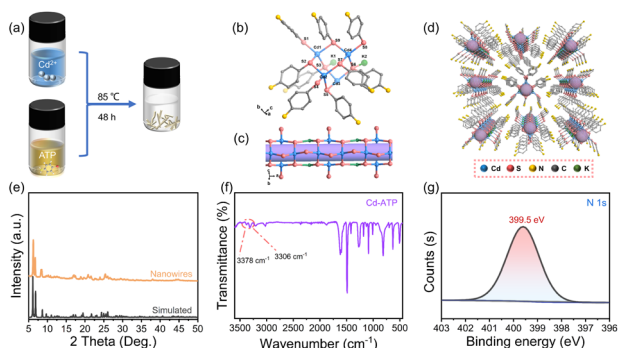


Fig. 1 Structure and characterization of Cd-ATP. (a) Schematic diagram of synthesis of the Cd-ATP single crystal. (b) Asymmetric unit of Cd-ATP (hydrogen atoms are omitted for clarity). (c) Inorganic chain of Cd-ATP. (d) Packing structure of Cd-ATP. (e) Powder X-ray diffraction (PXRD) pattern of Cd-ATP. (f) Fourier-transform infrared (FT-IR) spectrum of Cd-ATP nanowires. (g) X-ray photoelectron spectroscopy (XPS) of Cd-ATP nanowires.

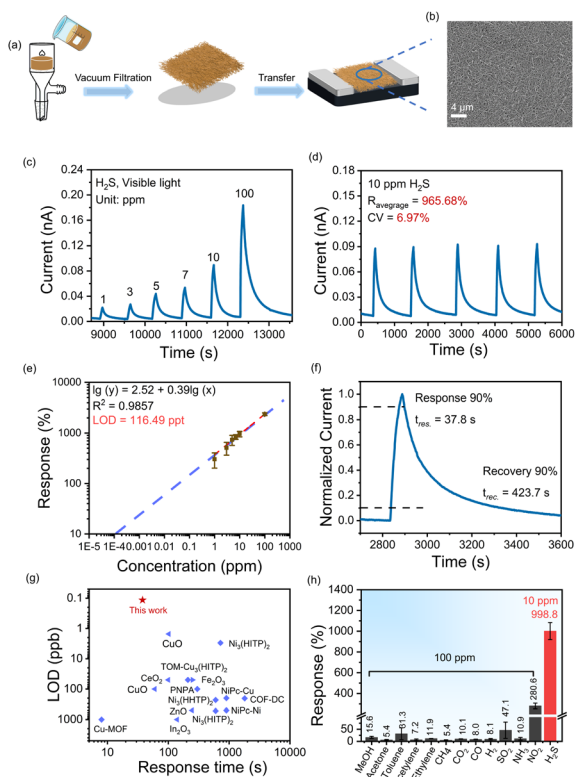


Fig. 3 Gas sensing performances of the devices at RT. (a) Process diagram of preparing Cd-ATP nanowire mesh films. (b) SEM of Cd-ATP nanowire mesh films. (c) Response of Cd-ATP to different H₂S concentrations under visible light. (d) Cycling stability to 10 ppm H₂S. (e) Linear double logarithmic curve of the response and concentration of Cd-ATP. (f) Response–recovery time curve of the Cd-ATP mesh film under 100 ppm H₂S. (g) Comparison with other pure materials at RT.³⁷ Data displayed in the graph were obtained or estimated from the corresponding cited reports. (h) Column chart of responses toward different gases of Cd-ATP nanowire mesh films.

The Cd-ATP mesh film shows a slight response (8.69%) when exposed to 100 ppm H₂S under dark conditions (Fig. S4†). It is worth mentioning that traditional cadmium chalcogenide-based nanowires have attracted wide attention due to their excellent visible-light-driven activity.³⁶ Cd-ATP mesh films also exhibit photoelectric response in visible light (420–760 nm) (Fig. S5†). The gas sensing properties of Cd-ATP have been greatly improved with the assistance of visible light (Fig. S6†). Under visible light conditions, Cd-ATP showed good response–recovery ability to a broad range of H₂S concentrations (1–100 ppm) with a light intensity of 360 K lx as shown in Fig. 3c. The current of the Cd-ATP mesh film distinctly increased when exposed to H₂S and recovered to the initial value after purging with air. The response of Cd-ATP mesh films toward 10 ppm H₂S was 965.68%, and the response coefficient of variation (CV) was only 6.97% over five continuous cycles (Fig. 3d), which indicated excellent repeatability. For 100 ppm H₂S, the response was up to 2296.42%, which is 264 times higher than that under dark conditions and 30 times higher than that of materials modified with polyaniline. The response–concentration log–log plots of Cd-ATP derived from Fig. 3e showed a good linear relationship

in the range of 1–100 ppm. The theoretical limit of detection (LOD) of Cd-ATP nanowire mesh films was 116.49 ppt by setting $R = 10\%$ (Fig. 3e). According to the response–recovery curve to 10 ppm H₂S, the response and recovery times of Cd-ATP nanowire mesh films can be estimated to be 37.8 and 423.7 s, respectively (Fig. 3f). Notably, the LOD value is lowest in all reported RT H₂S sensing non-composite materials (Fig. 3g and Table S3†). The fully covered –NH₂ group on the surface of Cd-ATP nanowires not only enhanced the sensitivity but also provided excellent selectivity to H₂S. As shown in Fig. 3h, Cd-ATP nanowire mesh films showed excellent selectivity to H₂S compared with other typical 12 interference gases, including acetone, NH₃, methylbenzene, CO₂, and SO₂, indicating that the Cd-ATP nanowire mesh film is capable of selectively distinguishing H₂S from its interference gases. Furthermore, the response value of Cd-ATP nanowire mesh film devices to 10 ppm H₂S does not decay obviously after storage for 15 days as illustrated in Fig. S7.† Furthermore, PXRD of Cd-ATP nanowire mesh film devices maintains good crystallinity and long-term stability after being exposed to H₂S. To verify the interference of water vapor in the environment, the response of Cd-ATP nanowire film devices to 10 ppm H₂S was tested at different humidity levels. The results show that for 10 ppm H₂S the response value of Cd-ATP nanowire films is 497% at 10% RH, and the response values do not change greatly at different humidity levels (Fig. S8†). The reduced response under different humidity may be due to partial dissolution of hydrogen sulfide in water. Although the response value is reduced, it still shows a certain response under humidity, so H₂S can be detected under the condition of different humidity.

In order to clarify the excellent gas-sensing performance of the gas sensors, *in situ* diffuse reflectance infrared Fourier transform spectroscopy (DRIFTS) (Fig. 4a) and electron paramagnetic resonance (EPR) (Fig. 4b) were performed to disclose the possible mechanism. When the Cd-ATP nanowire was in contact with H₂S, the H₂S molecules adsorbed on the surface of the nanowire through hydrogen bonding, which was confirmed

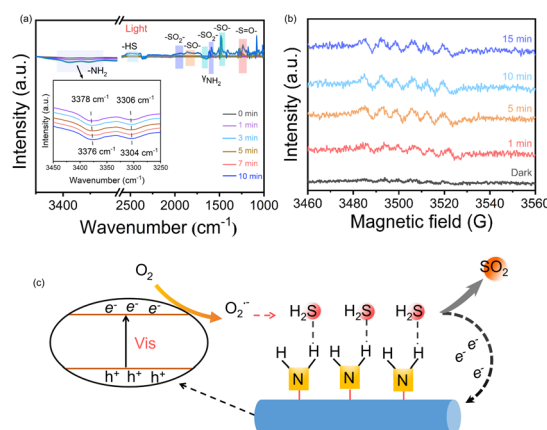


Fig. 4 (a) Time-resolved DRIFTS difference spectra of Cd-ATP. (b) Electron paramagnetic resonance (EPR) spectra of Cd-ATP nanowires in the dark and under light conditions. (c) The proposed sensing mechanism of Cd-ATP to H₂S.

by DRIFTS. The amino group stretching resonances of Cd-ATP nanowires are observed at 3378 and 3306 cm^{-1} under air conditions. And these peaks red shift to 3376 and 3304 cm^{-1} with increasing exposure time to the H_2S atmosphere, indicating the formation of a $\text{N}-\text{H}\cdots\text{S}$ hydrogen bond between the amino functional group and H_2S .^{38–43} Furthermore, the adsorption energy of hydrogen bonding was calculated based on the adsorption isotherms, and the adsorption energy of Cd-ATP nanowires for H_2S was 66.87 kJ mol^{-1} in the range of hydrogen bonding adsorption^{44,45} (Fig. S9†). Meanwhile, oxygen adsorbed on the surface of the nanowire is activated to superoxide radicals under visible light (Fig. 4b). Then, the superoxide radicals react with H_2S to produce SO_2 and release electrons into the material at the same time. Due to the N-type properties of Cd-ATP, the resistance of the material decreases and the current increases after receiving the extra electrons. The reaction of a superoxide radical with H_2S to produce SO_2 was confirmed by *in situ* DRIFTS (Fig. 4a). The strength of the out-of-plane stretching resonance band of the amino group was observed at 1624 cm^{-1} which decreased with increasing upon H_2S exposure time, indicating increasing interaction between $-\text{NH}_2$ and H_2S . Additionally, five new peaks, belonging to $-\text{SH}$ (2591 cm^{-1}), $-\text{S}-\text{O}-$ (1240 cm^{-1}), $-\text{SO}_2-$ (1162 cm^{-1}), and $-\text{S}=\text{O}-$ (1083 cm^{-1}), were observed, indicating the formation of SO_2 .^{46–50} Moreover, none of the peaks related to nitrates (1350 cm^{-1}) was detected, indicating that the amino group is not oxidized. The current of the Cd-ATP nanowire mesh film device gradually recovered to the baseline when re-purging with dry air. Following the principles of semiconductor sensors, it is speculated that surface amino functional groups and photo-induced superoxide radicals play an important role in transforming the surface disturbance into an electrical signal in the framework.^{51–53} In brief, the amino functional group on the surface selectively captures H_2S through hydrogen bonding interactions, making the material exhibit high selectivity. The superoxide radicals generated by light react with the captured H_2S to produce SO_2 and release electrons *via* Cd-ATP, causing an enhanced current and achieving highly sensitive detection.

Conclusions

In conclusion, a novel surface fully functionalized one-dimensional material was synthesized by a coordination self-assembly method. The Cd-ATP nanowire with a fully and orderly arranged amino group exhibits specific recognition of H_2S . A chemiresistive gas sensor based on Cd-ATP nanowire mesh films was demonstrated as a kind of designable high performance RT chemiresistive gas sensing material for the first time. This film exhibits the lowest LOD, very fast response and recovery, and excellent selectivity towards H_2S at RT under visible light among all reported H_2S sensing non-composite materials. The gas sensing mechanism showed that the photo-generated superoxide radical made the material highly sensitive to H_2S . This preparation strategy provides new avenues for designing multifunctional one-dimensional materials with rich surface chemistry and new electrical applications.

Author contributions

Ying-Xue Jin: synthesis, characterization studies of Cd-ATP, data curation, formal analysis, investigation, visualization, methodology and writing-original draft. Jie Chen: result analysis of MEMs. Yong-Jun Chen: result analysis of gas sensing. Wei-Hua Deng: mechanism exploration. Xiao-Liang Ye: result analysis and funding acquisition. Guan-E Wang: conceptualization, data curation, formal analysis, investigation, writing-original draft writing – review & editing, and funding acquisition. Gang Xu: conceptualization, formal analysis, investigation, writing & editing, project administration and funding acquisition.

Conflicts of interest

There are no conflicts to declare.

Acknowledgements

This work was supported by the National Natural Science Foundation of China (22171263, 21975254 and 22271281), Scientific Research and Equipment Development Project of CAS (YJKYQ20210024), Fujian Science & Technology Innovation Laboratory for Optoelectronic Information of China (2021ZR101) and Natural Science Foundation of Fujian Province (2021J02017, 2022J05088 and 2022J06032).

References

- 1 P. Yang, R. Yan and M. Fardy, *Nano Lett.*, 2010, **10**, 1529–1536.
- 2 L. Wang, H. Liu, J. Zhuang and D. Wang, *Small Sci.*, 2022, 20220036.
- 3 S. H. Lee, B. Lee, B. J. Kim, B. J. Jeong, S. Cho, H. E. Jang, H. H. Cho, J.-H. Lee, J.-H. Park, H. K. Yu and J.-Y. Choi, *ACS Sens.*, 2022, **7**, 1912–1918.
- 4 A. Machín, K. Fontánz, J. C. Arango, D. Ortiz, J. De León, S. Pinilla, V. Nicolosi, F. I. Petrescu, C. Morant and F. Márquez, *Materials*, 2021, **14**, 2609.
- 5 Z. Xiao, X. Wang, J. Meng, H. Wang, Y. Zhao and L. Mai, *Mater. Today*, 2022, **56**, 114–134.
- 6 Q. Lin, Y. Ye, L. Liu, Z. Yao, Z. Li, L. Wang, C. Liu, Z. Zhang and S. Xiang, *Nano Res.*, 2020, **14**, 387–391.
- 7 C. A. Huerta-Aguilar, S. N. Valdivieso, P. Thangarasu, C. A. Camacho-Olguín and I. A. Reyes-Dominguez, *Res. Chem. Intermed.*, 2017, **44**, 155–171.
- 8 S. G. Kumar, R. Kavitha and P. M. Nithya, *J. Environ. Chem. Eng.*, 2020, **8**, 104313.
- 9 P. Rastogi, F. Palazon, M. Prato, F. Di Stasio and R. Krahne, *ACS Appl. Mater. Interfaces*, 2018, **10**, 5665–5672.
- 10 C. Yuan, X. Wang, X. Yang, A. A. Alghamdi, F. A. Alharthi, X. Cheng and Y. Deng, *Chin. Chem. Lett.*, 2021, **32**, 2079–2085.
- 11 C. Li, M. Curreli, H. Lin, B. Lei, F. N. Ishikawa, R. Datar, R. J. Cote, M. E. Thompson and C. Zhou, *J. Am. Chem. Soc.*, 2005, **127**, 12484–12485.

- 12 Á. Kukovecz, K. Kordás, J. Kiss and Z. Kónya, *Surf. Sci. Rep.*, 2016, **71**, 473–546.
- 13 L. Wang, W. Liu, T. Wang and J. Ni, *Chem. Eng. J.*, 2013, **225**, 153–163.
- 14 L. Zhu, C. Feng, F. Li, D. Zhang, C. Li, Y. Wang, Y. Lin, S. Ruan and Z. Chen, *RSC Adv.*, 2014, **4**, 61691–61697.
- 15 B. T. Raut, M. A. Chougule, S. R. Nalage, D. S. Dalavi, S. Mali, P. S. Patil and V. B. Patil, *Ceram. Int.*, 2012, **38**, 5501–5506.
- 16 O. Veselska and A. Demessence, *Coord. Chem. Rev.*, 2018, **355**, 240–270.
- 17 Y. Li, X. Jiang, Z. Fu, Q. Huang, G.-E. Wang, W.-H. Deng, C. Wang, Z. Li, W. Yin, B. Chen and G. Xu, *Nat. Commun.*, 2020, **11**, 261.
- 18 X. Deng, S.-L. Zheng, Y.-H. Zhong, J. Hu, L.-H. Chung and J. He, *Coord. Chem. Rev.*, 2022, **450**, 214235.
- 19 G. E. Wang, S. Luo, T. Di, Z. Fu and G. Xu, *Angew. Chem., Int. Ed.*, 2022, **61**, e202203151.
- 20 Z. Wu, Q. Yao, Z. Liu, H. Xu, P. Guo, L. Liu, Y. Han, K. Zhang, Z. Lu, X. Li, J. Zhang and J. Xie, *Adv. Mater.*, 2021, **33**, 2006459.
- 21 X. Wang, Y. Lu, H. Zhao, Y. H. Sun and R. M. Wang, *Nanoscale*, 2021, **13**, 6921.
- 22 K. H. Low, C. H. Li, V. A. L. Roy, S. S. Y. Chui, S. L. F. Chana and C. M. Che, *Chem. Sci.*, 2010, **1**, 515–518.
- 23 H. Yu, P. Xiao, J. Tian, F. Wang and J. Yu, *ACS Appl. Mater. Interfaces*, 2016, **8**, 29470–29477.
- 24 X. H. Liu, P. F. Yin, S. A. Kulinich, Y. Z. Zhou, J. Mao, T. Ling and X. W. Du, *ACS Appl. Mater. Interfaces*, 2017, **9**, 602–609.
- 25 Y. Wen, G. E. Wang, X. Jiang, X. Ye, W. Li and G. Xu, *Angew. Chem., Int. Ed.*, 2021, **60**, 19710–19714.
- 26 H. Yuan, N. Li, W. Fan, H. Cai and D. Zhao, *Adv. Sci.*, 2022, **9**, e2104374.
- 27 Z. Li, Y. Guo, Z. Hu, J. Su, J. Zhao, J. Wu, J. Wu, Y. Zhao, C. Wu and Y. Xie, *Angew. Chem., Int. Ed.*, 2016, **55**, 8018–8022.
- 28 M. Sadakiyo, T. Yamada and H. Kitagawa, *J. Am. Chem. Soc.*, 2009, **131**, 9906–9907.
- 29 D. Wang, D. Zhang, Y. Yang, Q. Mi, J. Zhang and L. Yu, *ACS Nano*, 2021, **15**, 2911–2919.
- 30 D. Wang, D. Zhang and Q. Mi, *Sens. Actuators, B*, 2022, **350**, 130830.
- 31 D. Wang, D. Zhang, M. Tang, H. Zhang, T. Sun, C. Yang, R. Mao, K. Li and J. Wang, *Nano Energy*, 2022, **100**, 107509.
- 32 D. Wang, D. Zhang, Q. Pan, T. Wang and F. Chen, *Sens. Actuators, B*, 2022, **371**, 132481.
- 33 D. Wang, D. Zhang, M. Tang, H. Zhang, T. Sun, C. Yang, R. Mao, K. Li and J. Wang, *Nano Energy*, 2022, **100**, 107509.
- 34 D. Zhang, Z. Xu, Z. Yang and X. Song, *Nano Energy*, 2020, **67**, 104251.
- 35 Y. Yang, D. Zhang, D. Wang, Z. Xu and J. Zhang, *J. Mater. Chem. A*, 2021, **9**, 14495–14506.
- 36 D. Zhang, Y. e. Sun, C. Jiang, Y. Yao, D. Wang and Y. Zhang, *Sens. Actuators, B*, 2017, **253**, 1120–1128.
- 37 (a) A. Ali, H. H. D. ALTakroori, Y. E. Greish, A. Alzamy, L. A. Siddig, N. Qamhieh and S. T. Mahmoud, *Nanomaterials*, 2022, **12**(6), 913; (b) T. Lee, J. O. Kim, C. Park, H. Kim, M. Kim, H. Park, I. Kim, J. Ko, K. Pak, S. Q. Choi, I. D. Kim and S. Park, *Adv. Mater.*, 2022, **34**, 2107696; (c) M. Miao, Z. Wang, Z. Guo and J. Xing, *Adv. Mater. Interfaces*, 2022, **9**, 2101908; (d) Z. Meng, R. M. Stolz and K. A. Mirica, *J. Am. Chem. Soc.*, 2019, **141**, 11929–11937; (e) M. K. Smith and K. A. Mirica, *J. Am. Chem. Soc.*, 2017, **139**, 16759–16767; (f) V. V. Chabukswar, S. V. Bhavsar, A. S. Horne, K. Handore, V. B. Gaikwad and K. C. Mohite, *Macromol. Symp.*, 2013, **327**, 39–44; (g) Z. Meng, A. Aykanat and K. A. Mirica, *J. Am. Chem. Soc.*, 2018, **141**, 2046–2053; (h) N. S. Ramgir, S. K. Ganapathi, M. Kaur, N. Datta, K. P. Muthe, D. K. Aswal, S. K. Gupta and J. V. Yakhmi, *Sens. Actuators, B*, 2010, **151**, 90–96; (i) Y. Wang, G. Duan, Y. Zhu, H. Zhang, Z. Xu, Z. Dai and W. Cai, *Sens. Actuators, B*, 2016, **228**, 74–84; (j) Z. Li, X. Niu, Z. Lin, N. Wang, H. Shen, W. Liu, K. Sun, Y. Q. Fu and Z. Wang, *J. Alloys Compd.*, 2016, **682**, 647–653; (k) Y. Huang, W. Chen, S. Zhang, Z. Kuang, D. Ao, N. R. Alkurd, W. Zhou, W. Liu, W. Shen and Z. Li, *Appl. Surf. Sci.*, 2015, **351**, 1025–1033; (l) Z. Huang, X. Wang, F. Sun, C. Fan, Y. Sun, F. Jia, G. Yin, T. Zhou and B. Liu, *Mater. Des.*, 2021, **201**, 109507; (m) Z. S. Hosseini, A. I. zad and A. Mortezaali, *Sens. Actuators, B*, 2015, **207**, 865–871.
- 38 L. Cheng, Q. Xiang, Y. Liao and H. Zhang, *Energy Environ. Sci.*, 2018, **11**, 1362–1391.
- 39 C.-T. Lin, S.-W. Kuo, C.-F. Huang and F.-C. Chang, *Polymer*, 2010, **51**, 883–889.
- 40 L. Shen, G. Lei, Y. Fang, Y. Cao, X. Wang and L. Jiang, *Chem. Commun.*, 2018, **54**, 2475.
- 41 F. Sun, J. Liu, H. Chen, Z. Zhang, W. Qiao, D. Long and L. Ling, *ACS Catal.*, 2013, **3**, 862–870.
- 42 Y. J. Wang, X. N. Zhang, Y. Song, Y. Zhao, L. Chen, F. Su, L. Li, Z. L. Wu and Q. Zheng, *Chem. Mater.*, 2019, **31**, 1430–1440.
- 43 H. J. Zhang, T. L. Sun, A. K. Zhang, Y. Ikura, T. Nakajima, T. Nonoyama, T. Kurokawa, O. Ito, H. Ishitobi and J. P. Gong, *Adv. Mater.*, 2016, **28**, 4884–4890.
- 44 X. N. Zhang, Y. J. Wang, S. Sun, L. Hou, P. Wu, Z. L. Wu and Q. Zheng, *Macromolecules*, 2018, **51**, 8136–8146.
- 45 T. Steiner, *Angew. Chem., Int. Ed.*, 2002, **41**, 48–76.
- 46 T. Xu, P. Xu, D. Zheng, H. Yu and X. Li, *Anal. Chem.*, 2016, **88**, 12234–12240.
- 47 B. J. Lindberg, *Acta Chem. Scand.*, 1967, **21**, 2215–2234.
- 48 F. A. Cotton, R. Francis and W. D. Horrocks, *J. Phys. Chem.*, 1960, **64**, 1534–1536.
- 49 R. S. Drago and D. Meek, *J. Phys. Chem.*, 1961, **65**, 1446–1447.
- 50 E. D. Amstutz, I. M. Hunsberger and J. J. Chessick, *J. Am. Chem. Soc.*, 1951, **73**, 1220–1224.
- 51 J. Cui, L. Shi, T. Xie, D. Wang and Y. Lin, *Sens. Actuators, B*, 2016, **227**, 220–226.
- 52 B. Zu, Y. Guo and X. Dou, *Nanoscale*, 2013, **5**, 10693–10701.
- 53 W. Guo, J. Ma, G. Pang, C. Wei and W. Zheng, *J. Mater. Chem. A*, 2014, **2**, 1032–1038.